Density, distribution, and orientation of water molecules inside and outside carbon nanotubes

J. A. Thomas[a] and A. J. H. McGaughey[b]
Department of Mechanical Engineering, Carnegie Mellon University, Pittsburgh, Pennsylvania 15213, USA

(Received 7 November 2007; accepted 3 January 2008; published online 29 February 2008)

The behavior of water molecules inside and outside 1.1, 2.8, 6.9, and 10.4 nm diameter armchair carbon nanotubes (CNTs) is predicted using molecular dynamics simulations. The effects of CNT diameter on mass density, molecular distribution, and molecular orientation are identified for both the confined and unconfined fluids. Within 1 nm of the CNT surface, unconfined water molecules assume a spatially varying density profile. The molecules distribute nonuniformly around the carbon surface and have preferred orientations. The behavior of the unconfined water molecules is invariant with CNT diameter. The behavior of the confined water, however, can be correlated to tube diameter. Inside the 10.4 nm CNT, the molecular behavior is indistinguishable from that of the unconfined fluid. Within the smaller CNTs, surface curvature effects reduce the equilibrium water density and force water molecules away from the surface. This effect changes both the molecular distribution and preferred molecular orientations. © *2008 American Institute of Physics*.
[DOI: 10.1063/1.2837297]

I. INTRODUCTION AND MOTIVATION

Advances in carbon nanotube (CNT) fabrication techniques and new experimental and theoretical investigations into fluid flow through ultraconfined geometries have generated interest in nanofluidic based sensors and devices.[1] Yun *et al.* recently fabricated stable and axially aligned CNT arrays with an unprecedented length of 1 cm.[2] Li *et al.* built CNT networks containing well-aligned and uniform CNT Y-junctions with controllable branch and spur dimensions.[3] Skoulidas *et al.*[4] and Holt *et al.*[5] both reported anomalously high mass flow rates through CNT membranes, while Shim *et al.* functionalized CNT surfaces to be biocompatible and capable of recognizing proteins.[6]

The thermophysical and mass transport properties of such liquid-CNT systems—information necessary for device design and optimization—are related to the liquid-carbon intermolecular interactions and the associated surface wettability. These wetting characteristics can be implicitly incorporated into continuum-based analysis techniques by selecting appropriate boundary conditions for the mass, momentum, and energy transfer equations. For transport analysis at the nanoscale, however, where continuum assumptions break down,[7–9] explicit modeling of individual molecules is necessary to predict system performance.

The small length and time scales associated with atomic-level dynamics limit the ability of laboratory experiments to resolve liquid-CNT interactions. Molecular dynamics (MD) simulation, which can access these scales, has emerged as an alternative tool for studying such nanoscale transport phenomena.[10–18] In a MD simulation, intermolecular potential functions and the Newtonian equations of motion are used to calculate the position and momentum space trajectories of a system of molecules. The molecular behavior can then be used to predict thermophysical properties and study transport phenomena.

Predictions from MD simulations have indicated that the behavior of liquid water both inside and outside of CNTs is strongly influenced by interactions with the carbon atoms.[13–16] Walther *et al.* predicted a spatially varying density profile and nonuniform molecular orientation distribution in water outside a 12.5 nm single-walled CNT.[13] Similar variations in water density were predicted by Choundhury for water-C_{60} suspensions.[14] In investigating flow through single-walled CNTs, Kotsalis *et al.* predicted enhanced liquid ordering near the interior carbon surface and low liquid densities across the channel centerline.[15] Nonuniform interior water density profiles that vary as a function of CNT diameter were also reported by Hanasaki and Nakatani.[16]

To compliment these investigations and assist in the design of future nanofluidic devices, here we use MD simulations to systematically investigate the effect of CNT diameter on the density, distribution, and orientation of water molecules inside and outside single-walled 1.1, 2.8, 6.9, and 10.4 nm diameter armchair CNTs [with chirality vectors of (8,8), (20,20), (50,50), and (75,75)]. We go beyond previously reported simulation results by elucidating the specific molecular interactions responsible for the spatially varying liquid properties. We also identify how, in addition to liquid water density, tube diameter can passively tune the distribution and orientation of confined water molecules. Such information may be useful in understanding how water flows through and around CNTs, and how heat is transferred between a CNT and a surrounding liquid.

We begin by discussing the water-water and water-

[a]Electronic mail: jathomas@cmu.edu.
[b]Author to whom correspondence should be addressed. Electronic mail: mcgaughey@cmu.edu.

carbon intermolecular potential functions and the MD simulation techniques used to analyze the CNT-water system. Next, we study the effect of CNT diameter on liquid density both inside and outside the CNT. We then identify the effect of CNT diameter on the distribution of water molecules near the CNT surface and correlate these results to previously reported experimental measurements. Finally, we identify the molecular orientation distribution of water molecules both inside and outside the CNT and discuss how the orientation is affected by tube diameter.

II. MOLECULAR DYNAMICS SIMULATIONS SETUP

A. Water potential

We model water-water interactions using the TIP5P potential.[19] In TIP5P, each water molecule consists of one electrostatically neutral oxygen atom, two positively charged hydrogen atoms, and two negatively charged but massless interaction sites. The relative positions of the oxygen and hydrogen atoms correspond to known molecular structure data, while the positions of the charged interaction sites were tuned to reproduce the experimentally observed properties of bulk water.[19] The three atoms and two interaction sites are fixed with respect to a local basis set and each molecule has zero net charge.

The interaction between two water molecules, a and b, is a combination of one Lennard-Jones (LJ) interaction between the oxygen atoms, and 16 electrostatic interactions between the two hydrogen atoms and two charge sites on each molecule,

$$\phi_{ab} = 4\epsilon_{\mathrm{OO}}\left[\left(\frac{\sigma_{\mathrm{OO}}}{r_{\mathrm{OO}}}\right)^{12} - \left(\frac{\sigma_{\mathrm{OO}}}{r_{\mathrm{OO}}}\right)^{6}\right] + \sum_{i=1}^{4}\sum_{j=1}^{4}\frac{1}{4\pi\epsilon_0}\frac{q_i q_j}{r_{ij}}. \tag{1}$$

In Eq. (1), ϵ_{OO} and σ_{OO} are the LJ parameters for the oxygen-oxygen interaction, r_{OO} is the oxygen-oxygen separation distance, q_i is the charge on site i of molecule a, q_j is the charge on site j of molecule b, ϵ_0 is the permittivity of free space, and r_{ij} is the charge site separation distance. We use the potential parameters and charges recommended by the potential developers.[19]

As recommended in the original TIP5P implementation, we subject all molecular interactions to a 0.9 nm oxygen-oxygen cutoff radius at which interactions are truncated. It has been asserted that applying a spherical cutoff to a water model with long-range electrostatic interactions adversely effects system energetics and density.[20] To address this point, in Fig. 1 we show the net intermolecular force versus oxygen separation distance between two TIP5P water molecules in an equilibrated simulation of 512 molecules at a temperature of 298 K and a pressure of 1 atm. A range of forces (illustrated by the shaded envelope on the plot) are measured at each separation distance and are related to the variety of relative orientations accessible to the molecules. The mean effective intermolecular force at each distance is also shown. For two molecules separated by more than 0.7 nm, the force envelope decays as $1/(r_{\mathrm{OO}})^4$, characteristic of the interaction between two permanent dipoles.[21] The mean effective force

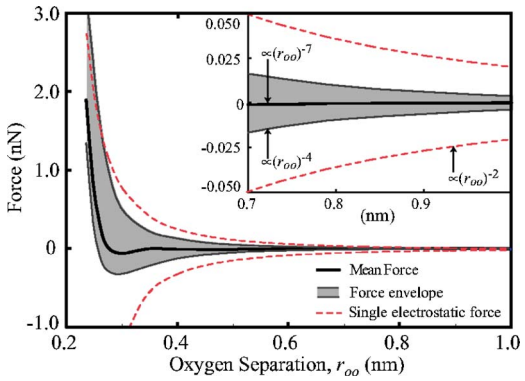

FIG. 1. (Color online) Intermolecular force vs oxygen separation distance between two water molecules in an equilibrated simulation of 512 molecules at a temperature of 298 K and a pressure of 1 atm. The gray envelope represents the range of forces predicted at each separation distance. The solid line is the mean force at each distance. Inset: force envelope and mean force at separation distances greater than 0.7 nm. At these separations, the force envelope decays as $1/(r_{\mathrm{OO}})^4$, characteristic of a permanent dipole–permanent dipole interaction. The mean effective force is related to the oxygen-oxygen LJ interactions and decays as $1/(r_{\mathrm{OO}})^7$.

at such separation distances (solid line) decays as $1/(r_{\mathrm{OO}})^7$, consistent with the oxygen-oxygen LJ interaction. Consequently, the total force between two molecules, which is used to integrate the equations of motion, decays much more rapidly than the individual Columbic forces [which decay as $1/(r_{\mathrm{OO}})^2$]. This rapid decay is why, even with truncating the individual long-range Coulomb interactions, the TIP5P model can accurately reproduce water statistics.[22] Along with the domination of nearest neighbor interactions on overall dynamics, this trend also explains why others have been able to successfully model water using even smaller truncation spheres.[23] Such a rapid decay in intermolecular forces will not be present in ionic systems where individual molecules have a nonzero charge.

B. Carbon-water potential

We model carbon-water interactions using the LJ potential recommended by Werder *et al.*,

$$\phi_{\mathrm{CO}} = 4\epsilon_{\mathrm{CO}}\left[\left(\frac{\sigma_{\mathrm{CO}}}{r_{\mathrm{CO}}}\right)^{12} - \left(\frac{\sigma_{\mathrm{CO}}}{r_{\mathrm{CO}}}\right)^{6}\right], \tag{2}$$

where r_{CO} is the carbon-oxygen separation distance, ϵ_{CO} $(=1.11\times10^{-21}$ J) is the depth of the LJ energy well, and σ_{CO} (=0.319 nm) is the LJ length scale.[24] A 0.9 nm cutoff is applied to the carbon-oxygen interactions. Although the CNT-water contact angle is not well defined from experiment,[25] the recommended parameters accurately reproduce the observed wetting behavior of water on graphite.

The LJ potential is a model of atomic repulsion due to overlapping electron orbitals and atomic attraction due to atomic dipole dispersion (i.e., van der Waals forces). The carbon atoms in a CNT are sp^2 hybridized, meaning that each carbon has one delocalized π-electron. Thus, in addition to carbon-oxygen LJ interactions and possible carbon-hydrogen interactions,[26] water molecules may also interact with this delocalized electron. Previous MD simulations have demonstrated that the electrostatic interactions between

a CNT and water are negligible compared to the van der Waals interactions, suggesting that electron-water interactions may be unimportant.[27] However, additional *ab initio* potential development and more research into the CNT-water contact angle will determine if more sophisticated intermolecular potentials are necessary.

For computational efficiency, the carbon atoms within each simulation cell are fixed. In an extension of our previously reported work on monatomic LJ solid-fluid interfaces,[28] we found that fixing the solid atoms had no detectable effect on the density, distribution, and diffusion characteristics of the interfacial liquid. Others have reported that fixing the carbon atoms has little effect on the dynamics of adjacent water.[24]

Although stable single-walled nanotubes with diameters greater than 1.5 nm are difficult to fabricate, we have found that molecular behavior near multiwalled nanotubes is indistinguishable from that near single-walled CNTs due to the short range of the carbon-water interactions. Thus, the results from our single-walled nanotube simulations can be applied to multiwalled nanotubes with similar interior or exterior dimensions.

C. Simulation implementation and data collection

Our simulations are performed in the *NVT* ensemble (constant mass, volume, and temperature). The rotational dynamics of the water molecules are modeled using the quadterion method and translational dynamics are integrated using the Verlet leapfrog scheme with a 0.5 fs time step.[11] The temperature is maintained at 298 K using a Berendsen thermostat and the volume of the simulation cell is tuned to recover a water density of 1000 kg/m^3 in regions far from the carbon surface. Periodic boundary conditions are imposed in all three directions.

To predict the equilibrium water density inside the 1.1, 2.8, and 6.9 nm CNTs, we simulated an open-ended sample of each nanotube in a large water bath at a temperature and pressure of 298 K and 1 atm. The bath density away from the tube was maintained at 1000 kg/m^3 and water molecules were able to freely diffuse across the open ends of the tube. After 250 ps, the number of molecules enclosed inside the tube became steady in time, allowing us to determine the equilibrium density. The CNTs used to generate all of the subsequently reported data span the entire simulation cell (thereby isolating the confined and unconfined fluids) and were initially filled with the number of molecules corresponding to this equilibrium density. Simulating the 10.4 nm CNT in a large water bath is computationally impractical. As such, we determined the equilibrium internal water density by predicting the pressure inside a 64 nm^3 cube centered within a nanotube of this size that spans the simulation cell. The number of molecules inside the CNT was tuned to recover a pressure of 1 atm within the cube. Applying this same technique to the 6.9 nm CNT generated an equilibrium water density within 1% of that predicted using the water-bath method.

In Fig. 2(a) we present a snapshot of the 2.8 nm CNT. We virtually partition the water into a sequence of shells concentric to the carbon surface. The thickness of each shell is 0.2 nm, which can sufficiently resolve spatial variations in the system while enclosing a statistically meaningful sample of water molecules. We identify each shell using its midpoint radial position r relative to the radial location of the CNT surface R_c. We sort molecules based on the oxygen atom location and position the shells such that the CNT surface is aligned with the shell boundary at $r=R_c$. The implementation of this layering scheme has no influence on the system dynamics. The shell-specific data presented throughout this report were then obtained by averaging the statistics of each shell over five data sets, with each set consisting of a 200 ps equilibration period followed by 250 ps of data collection.

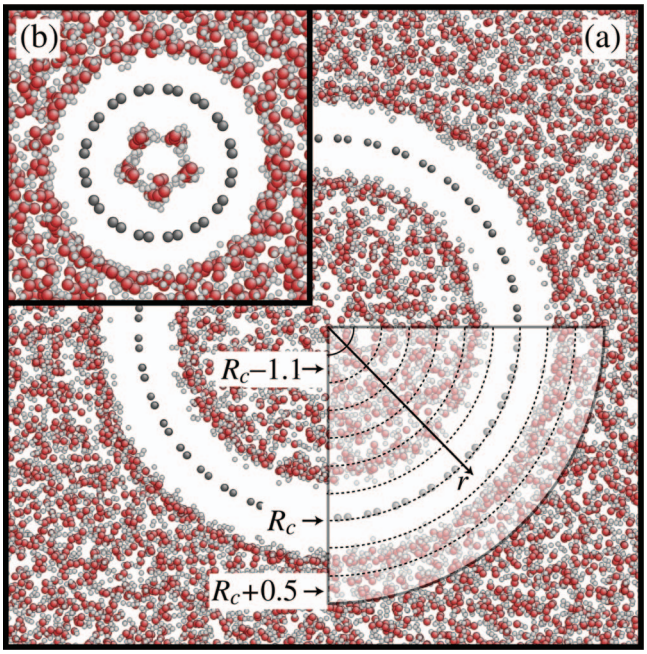

FIG. 2. (Color) (a) Cropped axial snapshot of 2.8 nm CNT in water. Full simulation cell side length is 7.5 nm. The layering scheme used to analyze water near and within the CNT is also shown. Each layer has a thickness of 0.2 nm and is identified using the midpoint radial position r. (b) Cropped axial snapshot of 1.1 nm CNT in water. Full cubic simulation cell side length is 5 nm. Both images are to the same scale and all numbers are in nanometers.

III. WATER DENSITY

Although the water molecules are continually moving, the time-averaged number of molecules within each liquid layer is well defined. Far from the CNT, the average number of molecules in each layer is spatially uniform and corresponds to the bulk density of 1000 kg/m^3. Closer to the CNT surface, as shown in Fig. 3, the unconfined water density is maximized at $r=R_c+0.3$ nm, minimized at $r=R_c+0.5$ nm, and slightly enhanced at $r=R_c+0.7$ nm. The density profiles within the unconfined water near each CNT are indistinguishable from what we found near a flat graphene sheet, implying that surface curvature has no effect on the radial density profile outside the CNT. In agreement with our predictions, scanning tunneling microscopy measurements of water on graphite reveal a distinct and dense water layer beginning 0.25 nm from the carbon surface.[29] Our findings

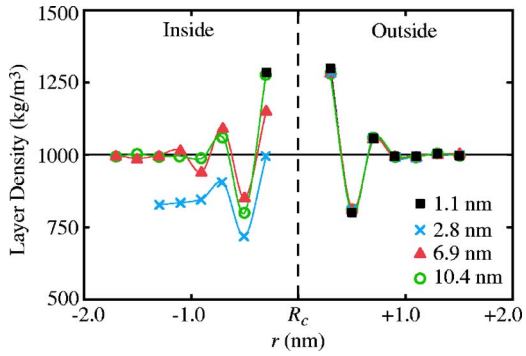

FIG. 3. (Color online) Water density inside and outside each CNT. The density profile in the unconfined water is invariant with CNT diameter and the same as that near a flat graphene sheet. The density profile in the confined water is a function of tube diameter. The innermost layers for the 1.1 and 2.8 nm tubes are at $r=R_c-0.3$ nm and $r=R_c-1.3$ nm. Guidelines are added to highlight the minima and maxima.

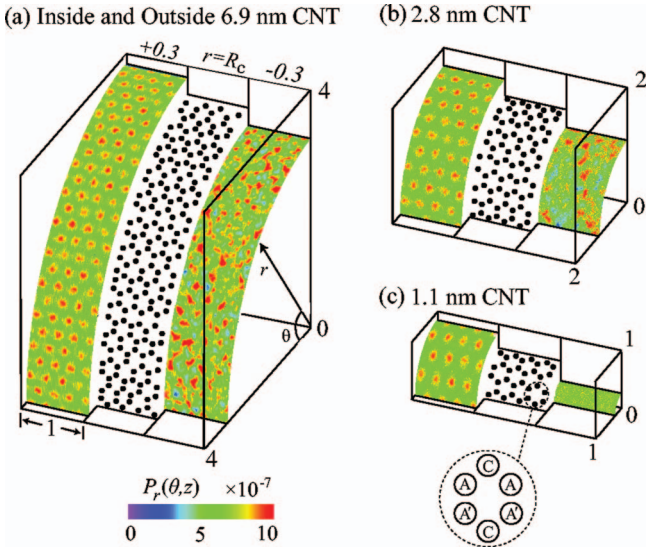

FIG. 4. (Color) [(a)–(c)] Molecular distribution at $r=R_c+0.3$ nm, $r=R_c$, and $r=R_c-0.3$ nm for the 6.9, 2.8, and 1.1 nm CNTs. The mass distribution at $r=R_c+0.3$ nm is similar for all tubes. For the 10.4 nm CNT, this same pattern is present at both $r=R_c-0.3$ nm and $r=R_c+0.3$ nm. The distribution at $r=R_c-0.3$ nm for the 6.9, 2.8, and 1.1 nm CNTs becomes more uniform with decreasing CNT diameter. In frame (c), the detailed view identifies the circumferentially aligned (C) and axially aligned carbon atoms (A and A′) that form the six-atom carbon honeycomb. All dimensions are in nanometers.

also agree with electronic structure calculations of water molecules near a flat graphite surface, which predict a water/graphite equilibrium separation distance of 0.32 nm.[30]

Similar density variations have been experimentally observed near the krypton-graphite interface[31] and predicted from MD simulation of liquid argon in a nanochannel.[28] This consistency suggests that although the current system includes electrostatic interactions, the density variations in the interfacial region are caused by the carbon-oxygen and oxygen-oxygen van der Waals interactions. At $r=R_c+0.3$ nm, the calculated carbon-oxygen potential energy due to LJ interactions is minimized, suggesting that the density maximum is indeed caused by oxygen atoms (and the associated water molecules) being drawn into an energetically favorable region near the carbon surface. At distances greater than $r=R_c+0.3$ nm, the carbon-oxygen LJ energy monotonically increases to zero and becomes too weak to directly influence water dynamics. Yet, the dense assembly of water molecules at $r=R_c+0.3$ nm extends the influence of the solid. At $r=R_c+0.5$ nm, 0.2 nm (one shell) beyond the water layer at $r=R_c+0.3$ nm, the calculated oxygen-oxygen interaction energy between water molecules is maximized. Thus, the dense layer at $r=R_c+0.3$ nm repels the molecules at $r=R_c+0.5$ nm, making the region energetically unfavorable and generating the density minimum seen in Fig. 3. The density enhancement at $r=R_c+0.7$ nm is then caused by attractive LJ interactions with the dense water layer at $r=R_c+0.3$ nm. This explanation seems reasonable given that the individual oxygen-oxygen LJ equilibrium separation distance, $2^{1/6}\sigma_{OO}$, is 0.36 nm.

Also presented in Fig. 3 is the density profile of the water confined inside each CNT. Unlike the exterior density profiles, the radial distribution of confined fluid molecules is strongly related to tube size. Water confined within the 10.4 nm CNT behaves much like the outside water, with similar density oscillations and a bulklike density of 1000 kg/m^3 recovered 1.0 nm from the solid surface. Inside the 6.9 nm tube, a bulklike water density of 1000 kg/m^3 is also recovered at the tube centerline. The density variations penetrate further into the liquid than those in the exterior interface, however, suggesting that surface curvature influences molecular behavior within the confined region as the CNT diameter decreases below 10 nm.

Inside the 2.8 nm CNT, the equilibrium water density at the tube centerline is 840 kg/m^3—significantly lower than the unconfined bulk density. Unlike in the larger tubes, where the 1 nm extent of surface effects is small compared to the tube diameter, the interface region within the 2.8 nm CNT is comparable to the tube diameter. The tube is too small to fully attenuate the influence of the solid and the confined water does not recover bulk properties. Thus, the behavior of water confined in a CNT becomes geometry dependent as the CNT diameter is decreased below 10 nm, consistent with the MD predictions of Koga and Tanaka for rectangular geometries[8] and Maniwa *et al.* for CNTs.[32] The water molecules inside the 1.1 nm CNT [see Fig. 2(b)] form a pentagon at $r=R_c-0.3$ nm with a density equivalent to that of the first exterior layer. Although some molecules diffuse across the channel centerline, the time-averaged number of particles outside this monolayer is very close to zero.

IV. WATER MOLECULE DISTRIBUTION

In addition to radial density variations, the distribution of water molecules around the CNT surface and along the tube axis varies with position. The water position probability distributions, $P_r(\theta,z)$, at $r=R_c+0.3$ nm and $r=R_c-0.3$ nm for the 6.9, 2.8, and 1.1 nm CNTs are shown in Figs. 4(a)–4(c). The surface shading indicates mass distribution. The carbon structure of each CNT at $r=R_c$ is also shown.

For all four nanotubes, water molecules at $r=R_c+0.3$ nm assume a pattered mass distribution which follows the hexagonal structure of the carbon surface. This nonuni-

form mass distribution agrees with the dynamic force microscopy measurements of Ashino *et al.*,[33] who found that the forces within the carbon honeycomb for a singled-walled CNT were 45% greater than those near the carbon atoms. They demonstrated that the strong interactions form a potential well centered within the carbon honeycomb structure shaped much like the circular distribution profiles presented in Fig. 4. Their measured well minimum is located 0.37 nm from the carbon surface, very close to the location of our predicted density maximum. Moreover, these authors conclude that van der Waals interactions are the dominate interatomic forces near the surface, supporting our earlier hypothesis.

In the confined region, $P_r(\theta,z)$ at $r=R_c-0.3$ nm becomes more uniform with decreasing CNT diameter. Inside the 10.4 nm CNT (not shown), molecules assume a distribution indistinguishable from that near the exterior interface, confirming that curvature effects within such large CNTs are negligible. Within the 6.9 nm CNT, the mass distribution likewise assumes a honeycomb structure following the CNT surface. Compared to the 10.4 nm CNT, however, the patterning in the 6.9 nm CNT is less prominent. Inside the 2.8 nm CNT, density enhancements are present near and within some carbon honeycombs while other potential wells remain unfilled. Finally, within the 1.1 nm CNT, the molecular positions are completely uncorrelated to the carbon structure.

These trends suggest that reducing the CNT diameter pinches the interior potential wells centered within the carbon honeycombs, thereby squeezing molecules out of the honeycomb structure and toward the CNT centerline. Unable to settle within the pinched potential well, the molecules at $r=R_c-0.3$ nm become more uniformly distributed with decreasing CNT diameter. This pinching mechanism also explains why the 10.4 and 6.9 nm CNTs, which both recover a bulklike 1000 kg/m^3 density across the tube centerline, have different interior water density profiles: since fewer water molecules fill the pinched potential wells inside the 6.9 nm CNT honeycombs, the radial density at $r=R_c-0.3$ nm is lower than that inside the 10.4 nm CNT. Squeezed further from the solid surface, however, the influence of the molecules at $r=R_c-0.3$ nm near the 6.9 nm CNTs penetrates deeper into the confined fluid and extends the influence of the solid. Consistent with this idea, we have also found that with decreasing CNT diameter, the first peak of the carbon-oxygen radial distribution function inside the tube is located further from the carbon surface.

V. WATER MOLECULE ORIENTATION

To predict the influence of solid-liquid interactions on water molecule orientation, we calculate the unit dipole moment vector of all molecules with respect to the CNT surface normal. The vectors for all atoms in a given layer are then mapped onto a single unit sphere to form a layer-specific orientation distribution. In layers far from the surface, where interactions with the solid are fully attenuated, the molecular orientation distribution is uniform. At $r=R_c+0.3$ nm and $r=R_c-0.3$ nm, however, the molecules take on preferred orientations.

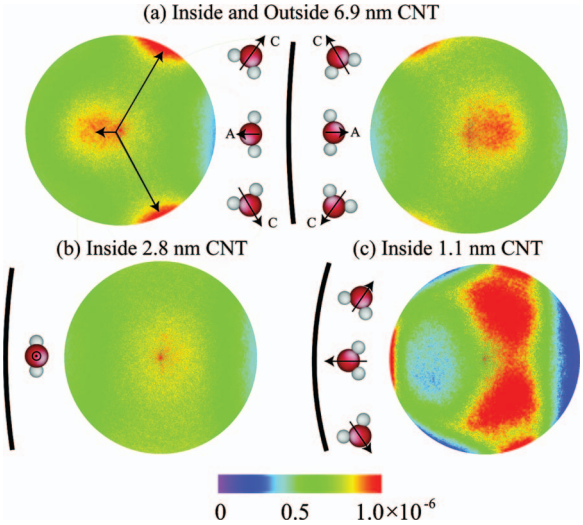

FIG. 5. (Color) (a) Orientation distribution spheres at $r=R_c+0.3$ and $r=R_c-0.3$ nm for the 6.9 nm CNT. The projected length of the unit dipole moment vector, as printed in the figure, indicates the degree of rotation out of the plane of the page. Molecules are biased toward either an axially aligned carbon atom (A) or a circumferentially aligned carbon atom (C), as highlighted by the orientation distribution and the three water molecules beside the sphere. (b) Orientation distribution at $r=R_c-0.3$ nm near the 2.8 nm CNT. A single preferred orientation points normal to (in or out of) the page. (c) Distribution at $r=R_c-0.3$ nm near the 1.1 nm CNT. The water molecules form a pentagonal structure, resulting in two preferred orientations pointing away from the surface. A third preferred orientation points toward the CNT surface but is unbiased toward any particular axially or circumferentially aligned carbon atom.

The orientation distribution map of water molecules at $r=R_c+0.3$ nm for the 6.9 nm CNT is shown in Fig. 5(a). Similar behavior is observed outside all four CNTs. Although all orientations are accessible to molecules in this layer, the molecules are most likely to point in one of three preferred directions. To understand this behavior, recall from Fig. 4 that water molecules are likely to reside in the potential well formed by the six-atom carbon honeycomb structure. As shown in Fig. 4(c), one pair of carbon atoms are axially aligned and two pairs of carbon atoms are circumferentially aligned. Although this symmetric arrangement generates a near circular potential well, water molecules within the potential well tend to point toward either a circumferentially aligned carbon atom (C) or an axially aligned carbon atom (A or A′).

The orientation distribution maps of water molecules at $r=R_c-0.3$ nm for the 6.9, 2.8, and 1.1 nm CNT are shown in Figs. 5(a)–5(c). Although not presented here, we note that the molecules at $r=R_c-0.3$ nm for the 10.4 nm nanotube orient like those at $r=R_c+0.3$ nm but mirrored toward the CNT surface. At $r=R_c-0.3$ nm for the 6.9 nm CNT, the water molecules are still likely to align with the CNT centerline axis but, compared to the 10.4 nm CNT, less likely to point toward a specific circumferentially aligned carbon atom. This trend continues in the 2.8 nm CNT, where water molecules at $r=R_c-0.3$ nm remain aligned with the CNT centerline axis, but have no affinity toward any particular circumferentially

aligned carbon atom. These correlations between orientation distribution and CNT diameter support the squeezing mechanism discussed earlier. As an increasing fraction of water molecules are squeezed out of the carbon honeycomb potential well, distinct interactions with the circumferentially aligned carbon pair become less pronounced. Thus, with decreasing CNT diameter, interactions between water and specific circumferentially aligned carbon atoms are less distinct and water molecules are instead spread over an increasing range of orientations. A preferred orientation remains in the direction of the axially aligned carbon atoms, however, since these atomic positions are unaffected by surface curvature. For the 1.1 nm CNT, the molecules are fully squeezed from the surface potential wells and two preferred orientations point away from the carbon surface. The orientation distribution is now governed by water-water interactions, forming the pentagonal arrangement illustrated in Fig. 2(b) and manifested in the orientation distribution. Unique molecular orientation distributions inside sub-2 nm CNTs were also reported by Koga *et al.*[34]

VI. SUMMARY AND CONCLUSION

We have investigated the effect of tube diameter on the density, molecular distribution and molecular orientation of water inside and outside single-walled CNTs. As presented in Figs. 3 and 4, the density of unconfined water molecules is enhanced and the molecular distribution is nonuniform near the carbon surface. This behavior is caused by water molecules moving to low-energy potential wells formed near the hexagonal carbon surface. The behavior of unconfined water molecules is invariant with CNT diameter. Inside the tube, however, curvature effects influence the molecular density and distribution near the CNT wall. The curved surface pinches the low-energy potential wells, thereby squeezing water molecules away from the carbon surface and decreasing the liquid density.

In addition to density and molecular distribution, interactions with the CNT influence the orientation of water molecules near the carbon surface. As presented in Fig. 5, the unconfined water molecules close to a CNT of any diameter are likely to point towards either a circumferentially or axially aligned carbon atom. Water molecules confined within the 10.4 and 6.9 nm CNTs orient much like unconfined water molecules. Inside the 2.8 nm CNT, where surface curvature effects are more relevant, water molecules are only likely to point towards axially aligned carbon atoms. Inside the 1.1 nm CNT, the molecular orientation is governed by water-water interactions and molecules have no affinity toward any particular carbon atom.

Tersoff and Ruoff predicted that van der Waals attraction between CNTs with diameters greater than 2.5 nm would cause the tubes to flatten against each other and form hexagonal cross sections.[35] López *et al.* have observed this so-called polygonization experimentally.[36] Inside our 2.8 nm CNT, where the water molecules do not recover bulklike properties, polygonization may influence the behavior of the confined fluid. Inside larger tubes, where bulklike properties are recovered, polygonization is unlikely to have an effect. Such bundling is likely to influence the behavior of water molecules in the interstitial region between two or more clustered CNTs.

The reduced influence of solid-water interactions on molecular orientation and distribution as the tube diameter gets smaller may be responsible for the high mass flow rates reported for water through 0.81 nm CNTs.[5,9] This behavior also suggests that thermal energy exchange between a CNT and surrounding fluid may be affected by tube diameter.[37]

[1] G. Gruner, Anal. Bioanal. Chem. **384**, 322 (2006).
[2] Y. Yun, Z. Dong, V. N. Shanov, A. Bange, W. R. Heineman, H. B. Halsall, L. Conforti, A. Bhattadharya, and M. J. Schulz, Proc. SPIE **6528**, 65280T (2007).
[3] J. Li, C. Papadopoulos, and J. Xu, Nature (London) **402**, 253 (1999).
[4] A. I. Skoulidas, D. M. Ackerman, J. K. Johnson, and D. S. Sholl, Phys. Rev. Lett. **89**, 185901 (2002).
[5] J. K. Holt, H. G. Park, Y. Wang, M. Stadermann, A. B. Artyukhin, C. P. Grigoropoulos, A. Noy, and O. Bakajin, Science **312**, 1034 (2006).
[6] M. Shim, N. W. S. Kam, R. J. Chen, Y. Li, and H. Dai, Nano Lett. **2**, 285 (2002).
[7] J. Martí and M. C. Gordillo, Phys. Rev. E **64**, 021504 (2001).
[8] K. Koga and H. Tanaka, J. Chem. Phys. **122**, 104711 (2005).
[9] G. Hummer, J. C. Rasaiah, and J. P. Noworyta, Nature (London) **414**, 188 (2001).
[10] E. S. Landry, S. Mikkilineni, M. Paharia, and A. J. H. McGaughey, J. Appl. Phys. **102**, 124301 (2007).
[11] M. P. Allen and D. J. Tildesley, *Computer Simulation of Liquids* (Oxford University Press, New York, 1987).
[12] R. S. Taylor, L. X. Dang, and B. C. Garrett, J. Phys. Chem. **100**, 11720 (1996).
[13] J. H. Walther, R. L. Jaffe, T. Halicioglu, and P. Koumoutsakos, J. Phys. Chem. B **107**, 1345 (2003).
[14] N. Choudhury, J. Phys. Chem. C **111**, 2565 (2007).
[15] E. M. Kotsalis, J. H. Walther, and P. Koumoutsakos, Int. J. Multiphase Flow **30**, 995 (2004).
[16] I. Hanasaki and A. Nakatani, J. Chem. Phys. **124**, 144708 (2006).
[17] J. Zou, B. Ji, X.-Q. Feng, and H. Gao, Small **2**, 1348 (2006).
[18] Y. Maniwa, H. Kataura, M. Abe, A. Udaka, S. Suzuki, Y. Achiba, H. Kira, K. Matsuda, H. Kadowaki, and Y. Okabe, Chem. Phys. Lett. **401**, 534 (2005).
[19] M. W. Mahoney and W. L. Jorgensen, J. Chem. Phys. **112**, 8910 (2000).
[20] M. Lísal, J. Kolafa, and I. Nezbeda, J. Chem. Phys. **117**, 8892 (2002).
[21] D. J. Griffiths, *Introduction to Electrodynamics*, 3rd ed. (Prentice Hall, New Jersey, 1999).
[22] M. W. Mahoney and W. L. Jorgensen, J. Chem. Phys. **114**, 363 (2001).
[23] W. L. Jorgensen and J. Tirado-Rives, Proc. Natl. Acad. Sci. U.S.A. **102**, 6665 (2005).
[24] T. Werder, J. H. Walther, R. L. Jaffe, T. Halicioglu, and P. Koumoutsakos, J. Phys. Chem. B **107**, 1345 (2003).
[25] A. H. Barber, S. R. Cohon, and H. D. Wagner, Phys. Rev. B **71**, 115443 (2005).
[26] R. L. Jaffe, P. Gonnet, T. Werder, J. H. Walther, and P. Koumoutsakos, Mol. Simul. **30**, 205 (2004).
[27] F. Moulin, M. Devel, and S. Picaud, Phys. Rev. B **71**, 165401 (2005).
[28] J. A. Thomas and A. J. H. McGaughey, J. Chem. Phys. **126**, 034707 (2007).
[29] G. Nagy, J. Electroanal. Chem. **409**, 19 (1996).
[30] D. Feller and K. D. Jordan, J. Phys. Chem. A **104**, 9971 (2000).
[31] R. F. Hainsey, R. Gangwar, J. D. Shindler, and R. M. Suter, Phys. Rev. B **44**, 3365 (1991).
[32] Y. Maniwa, H. Kataura, M. Abe, S. Suzuki, Y. Achiba, H. Kira, and K. Matsuda, J. Phys. Soc. Jpn. **71**, 2863 (2002).
[33] M. Ashino, A. Schwarz, T. Behnke, and R. Wiesendanger, Phys. Rev. Lett. **93**, 136101 (2004).
[34] K. Koga, G. T. Gao, H. Tanaka, and X. C. Zeng, Nature (London) **412**, 802 (2001).
[35] J. Tersoff and R. S. Rubio, Phys. Rev. Lett. **76**, 676 (1994).
[36] M. J. López, A. Rubio, J. A. Alonso, L.-C. Qin, and S. Iijima, Phys. Rev. Lett. **86**, 3056 (2001).
[37] S. Shenogin, L. Xue, R. Ozisik, P. Keblinski, and D. G. Cahill, J. Appl. Phys. **95**, 8136 (2004).